Nanoscale

PAPER

View Article Online
View Journal | View Issue

Cite this: *Nanoscale*, 2018, **10**, 4406

Stable, small, specific, low-valency quantum dots for single-molecule imaging†

Jungmin Lee,‡[a] Xinyi Feng,[b] Ou Chen,[c] Moungi G. Bawendi*[a] and Jun Huang*[b]

Received 20th November 2017,
Accepted 21st January 2018

DOI: 10.1039/c7nr08673c

rsc.li/nanoscale

We have developed a strategy for synthesizing immediately activable, water-soluble, compact (~10–12 nm hydrodynamic diameter) quantum dots with a small number of stable and controllable conjugation handles for long distance delivery and subsequent biomolecule conjugation. Upon covalent conjugation with engineered monovalent streptavidin, the sample results in a population consisting of low-valency quantum dots. Alternatively, we have synthesized quantum dots with a small number of biotin molecules that can self-assemble with engineered divalent streptavidin *via* high-affinity biotin–streptavidin interactions. Being compact, stable and highly specific against biotinylated proteins of interest, these low-valency quantum dots are ideal for labeling and tracking single molecules on the cell surface with high spatiotemporal resolution for different biological systems and applications.

Introduction

Fluorescence microscopy has made significant progress in biology with the development of fluorescent dyes and proteins in the recent decades.[1,2] However, the inherent problems of these two classes of labeling molecules are that they are less bright and liable to photobleaching.[3–5] Imaging many complex processes requires a bright, small, and photostable fluorescent probe with versatile optical properties.[5–7] Quantum dots (QDs), which are semiconductor nanoparticles, have been used widely to complement conventional organic dyes and fluorescent proteins due to their photostability, brightness, broad absorption, and narrow emission.[4–16] However, most immediately available QDs are large in size (~20–30 nm hydrodynamic diameter)[17–19] and incapable of precise, valency-controlled labeling of proteins of interest (POIs). Thus, the construct size and multivalency of labeling pose two major challenges when using QDs as fluorescent probes.[20–23]

To harness the attractive optical properties of QDs, it would be ideal to minimize their size and binding valency, preferably making them monovalent. The route of preparation for QDs, which is completely different from that for dyes or fluorescent proteins, relies heavily on organic ligands.[24,25] QDs need to be passivated with a ligand that renders the nanoparticles soluble in aqueous media.[26,27] The same ligand also needs to provide QDs with the ability to conjugate a biomolecule that targets the POI. Previously, we demonstrated that passivation with poly-imidazole ligands (PILs) results in stable water-solubilized QDs that can be conjugated to targeting biomolecules.[28] QD passivation and water-solubilization is followed by a reaction of amines on the ligands with *N*-hydroxysuccinimide- (NHS-) or maleimide-activated biomolecules. However, this conjugation sequence presents two problems. First, some of the amines stay unreacted due to the interaction of amines with the QD surface and second, polyethylene glycol (PEG) groups, often used as water-solubilizing moieties on the ligands, make amines even more inaccessible to the NHS reaction by creating steric hindrance between the amines on the QD surface and the biomolecules. Ultimately, these two factors together decrease the NHS reaction yield, and these unreacted amines later contribute to nonspecific binding to various surfaces other than the POI.[28] The low conjugation yield also makes it difficult to control the valency of targeting biomolecules per QD due to the large number of amines needed. An excess number of handles per QD may result in the aggregation of the POI, which may have inadvertent consequences such as turning on biological pathways *via* crosslinking. Yet another issue with NHS- and maleimide-activating schemes is that both groups are unstable even in moderately basic aqueous media (half-life = 10 min and 6 h at pH 8.5–8.6, respectively), limiting any long distance delivery of conjugable, water-soluble QDs from chemists to biologists for subsequent bio-

[a]*Department of Chemistry, Massachusetts Institute of Technology, USA. E-mail: mgb@mit.edu*
[b]*Institute for Molecular Engineering, University of Chicago, USA. E-mail: huangjun@uchicago.edu*
[c]*Department of Chemistry, Brown University, 324 Brook St., Providence, RI 02912, USA*

†Electronic supplementary information (ESI) available: Supplementary information and supplementary videos S1–S3. See DOI: 10.1039/c7nr08673c

‡Current address: Bioverativ Inc., 225 2nd Ave., Waltham, MA 02451, USA.

molecule conjugation and imaging applications. This stability problem persists for innovative conjugation chemistries such as norbornene–tetrazine chemistry,[29,30] highlighting the need for a strategy that increases the efficiency of amine conversion into a stable species that can easily be rendered reactive. One study has conjugated QDs with monovalent streptavidin (mSA) and purified monovalent QDs using agarose gel electrophoresis.[17] However, the particular method used for separating monovalent QDs has been found to be tedious and difficult due to its harsh treatment involving heat and centrifugation. Also, the conjugation relies on a reversible attachment of the 6-histidine tag (6×His-tag) of an mSA onto a QD surface, which is a non-covalent interaction and liable to dissociation. Ideally, a chromatography-based separation of constructs that have different valencies would provide quantitative and easy characterization. A later study has used phosphorothioate DNA of a defined length to prepare monovalent QDs based on the affinity of phosphorothioates for semiconductor surfaces.[31] However, such affinity-based conjugation may not be suitable for a complex cellular environment where DNase may digest the DNA wrapped on a QD and disrupt the labeling.[32–34] Also, the negative charge of the DNA on QDs could cause significant nonspecific binding.[35,36] DNA has also been employed to couple proteins in a stoichiometric and controlled manner onto QDs, by developing a peptide-modified tetrahedral DNA cage,[37] or using DNA hybridization for flexible and reliable conjugation.[38] Another alternative is to use zwitterionic ligands such as sulfobetaine with rigid conformations and increased exposure of the terminal ligands on the QD surface,[39] though precise controlling of QD binding valency remains to be developed.

Results and discussion

QD construct and bioconjugation strategy

Here we have developed a new method to make small, stable, specific, low-valency QDs for biological applications. Stable and immediately activable QDs without nonspecific binding to biomolecules were prepared by converting the amines on PILs into a protected, reactive group prior to ligand exchange and QD water-solubilization. Briefly, amine-containing PILs were reacted with succinimidyl 3-(2-pyridyldithio)propionate (SPDP), purified, and exchanged with the native hydrophobic ligands on the surface of CdSe/CdS core–shell QDs (Fig. 1a). The PILs provide stable multidentate imidazole binding motifs to the QD surface, offering a superior stability of the entire construct for further surface functionalization and biological applications.[40] This new procedure addressed the issues of low stability, high nonspecific binding and low biomolecule-coupling efficiency because the amines on the PIL were converted to a different chemical group that does not interact with the QD

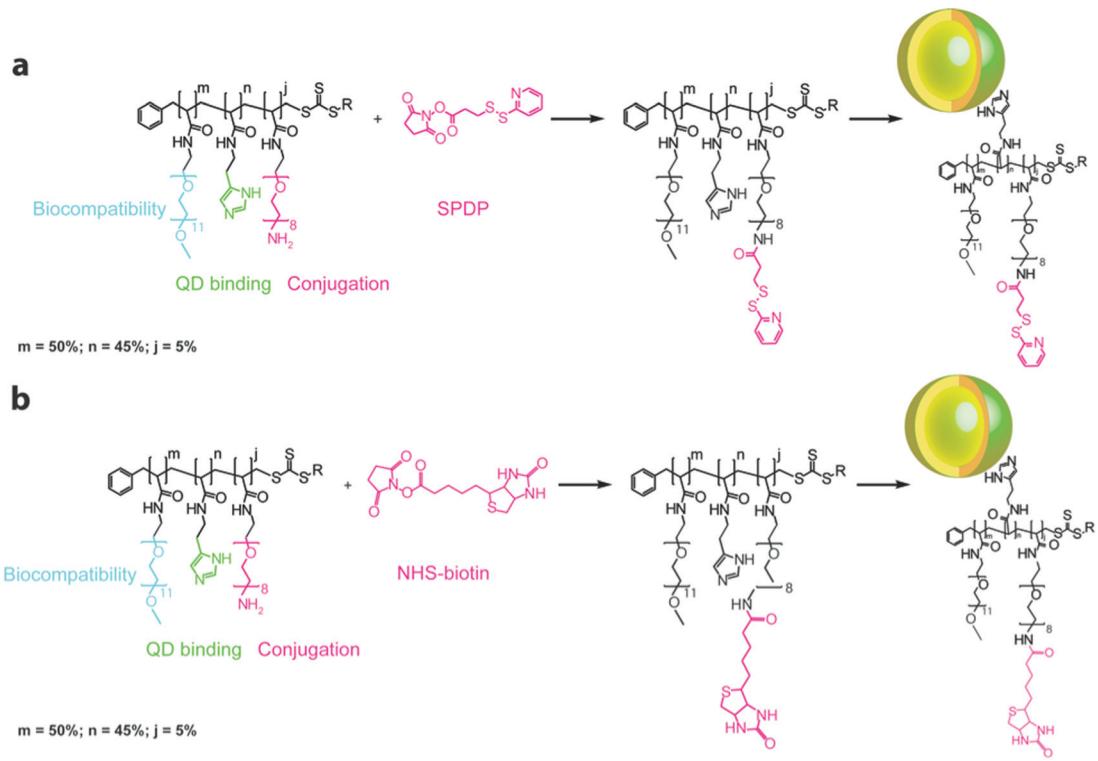

Fig. 1 Schematic of QD construct synthesis. (a) To make 5% SPDP–QDs, poly-imidazole ligands (PILs) containing methoxy-terminated poly(ethylene glycol)$_{11}$ (mPEG$_{11}$), imidazole, and amine-terminated poly(ethylene glycol)$_8$ (AminoPEG$_8$) groups were conjugated to SPDP prior to the ligand exchange with native hydrophobic ligands on the QD surface. (b) To make 5% biotin–QDs, AminoPEG$_8$-PILs were reacted with NHS-biotin, purified, and exchanged with the native ligands on the QD surface, allowing self-assembly with streptavidin molecules for immediate labeling and detection.

surface. By converting amines *a priori*, without the presence of the competing QD surface, we could minimize the number of amines required per PIL to 5% of the imidazole and PEG-based monomer units on the PIL. In previous conventional methods,[28] 25% amine units were required because some portion of the amine groups would become inaccessible for reactivity post QD–ligand exchange. This raised the risk of unreacted amines contributing positive charges to the nanoparticle overall, resulting in nonspecific binding.[28] Reducing the number of amines per QD by five-fold suggested that the nonspecific binding could be banished. Meanwhile, the ease and high efficiency of amine conversion greatly increased the biomolecule-coupling efficiency. In the meantime, we made a 5% biotin–QD construct using similar chemistry (Fig. 1b). Amine-containing PILs were reacted with *N*-hydroxysuccinimidobiotin (NHS-biotin), purified, and exchanged with the native ligands on the QD surface, allowing self-assembly with streptavidin molecules for immediate labeling and specific detection.

As expected, the 5% SPDP–QD construct maintained broad absorption and narrow emission bandwidths (Fig. 2a) and a compact hydrodynamic diameter of ~10–12 nm (Fig. 2b), which was determined from the elution time of gel filtration chromatography (GFC) performed on the QDs.[41,42] To verify the number of reactive groups on QDs, SPDP–QDs were deprotected to expose the thiol groups and subsequently reacted with maleimide-activated fluorescent dyes. The number of dyes per QD was calculated by separately determining the molar concentrations of the QDs and of the dyes based on absorbance measurements. The new procedure resulted in 5% SPDP–QDs that could react with a maximum of 6.20 maleimide dyes (Fig. 2c), compared to 0.66 when using 5% SPDP–QDs prepared by first coating the QDs with AminoPEG-PIL[28] and then reacting the amines with SPDP (ESI Fig. 1†). In other words, our new protocol produced SPDP–QDs with drastically improved potential reactivity, increasing the number of dyes conjugated per QD by 9.4 times (ESI Fig. 2†). Moreover, the presence of free amines on the nanoparticle surfaces has been found to cause nonspecific binding,[29] so our new protocol has potential to greatly enhance targeting specificity. In addition, our use of protected pyridylthiol groups as the QD conjugation handle addressed the issue of the stability of an activated QD. As shown in Fig. 2d, the number of maleimide dyes that can

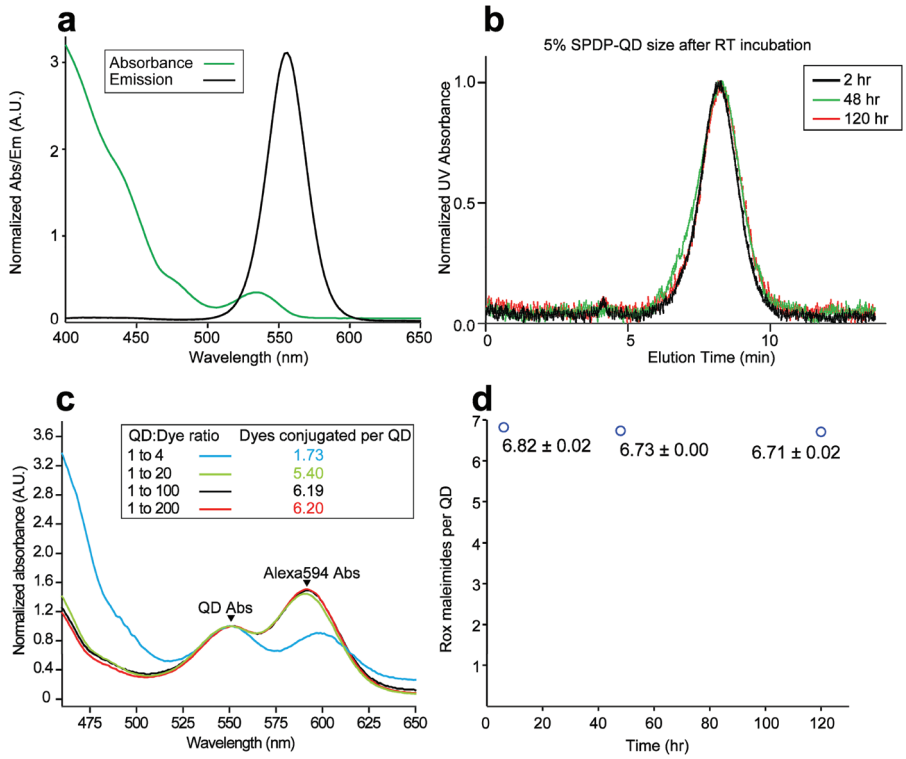

Fig. 2 Characterization of SPDP–QDs. (a) The broad absorbance and narrow emission bands of QD570 that has been ligand exchanged with PILs containing SPDP. (b) Size of SPDP–QDs after various hours of incubation at room temperature as measured by gel filtration chromatography (GFC). Symmetric GFC elution peaks at ~8.2 min correspond to an unaggregated, monodisperse QD solution of 10–12 nm hydrodynamic diameter. (c) Verification of the average number of SPDP per QD by saturating with incremental equivalents of maleimide-Alexa594 (Alexa594 absorption coefficient at 588 nm = 96 000 M^{-1} cm^{-1}, QD absorption coefficient at 350 nm = 1.53 × 10^6 M^{-1} cm^{-1}). The maximum number of conjugated dyes is 6 per QD. (d) Stability of thiol reactivity on SPDP–QDs in Dulbecco's modified Eagle's medium at room temperature, as measured by the number of maleimide dyes that can be conjugated. SPDP–QDs were stirred on a stir plate at 25 °C and aliquots were taken at 2, 48, and 120 h. Each aliquot was reacted first with dithiothreitol (DTT) to deprotect pyridylthiol groups, and then with an excess of maleimide dyes. The dye to QD ratio was calculated by measuring the absorbance at 575 nm (Rox absorbance peak, absorption coefficient at 575 nm = 82 000 M^{-1} cm^{-1}) and at 350 nm (QD absorbance, absorption coefficient at 350 nm = 1.53 × 10 M^{-1} cm^{-1}).

be conjugated per QD almost remained constant over the course of 120 hours (or 5 days) at room temperature. The high level of stability allows the optimized, homemade, reactive QDs to be transported *via* long distance delivery.

Conjugation of proteins to QDs

Next, we prepared chimeric streptavidin proteins and used them for testing conjugation with the synthesized QDs. We generated and purified a monovalent streptavidin (mSA) and a divalent streptavidin (dSA) with a cleavable 6×His-tag in the alive subunit. To obtain streptavidin with different valencies, we first mixed alive and dead streptavidin subunits at a 1 : 3 ratio. The protein mixture was then passed through a nickel column and eluted with imidazole, dialyzed, and finally purified using fast protein liquid chromatography (FPLC). After collection of different resulting streptavidin constructs and verification of their binding valencies (ESI Fig. 3†), the 6×His-tag was removed from mSA and dSA using the TEV protease to avoid interference with QD binding.

We then first conjugated the mSA to 5% SPDP–QDs. As illustrated in Fig. 3a, the 6×His-tag free mSA was activated using sulfosuccinimidyl-4-(*N*-maleimidomethyl)cyclohexane-1-carboxylate (Sulfo-SMCC) and the SPDP handles on the QDs were cleaved using dithiothreitol (DTT). After desalting twice with 7 kDa Zeba Spin Desalting Columns to remove Sulfo-SMCC and DTT, the sulfhydryl-reactive maleimide on the mSA reacted with the sulfhydryl group on the QDs to yield specific covalent-linked mSA–QD conjugates. The product was purified using FPLC with an S200 gel filtration column to remove the unconjugated mSA based on the size. Our previous experiments on the conjugation of small Alexa594 dyes (<1 kDa) to QDs have proved that the maximum number of SPDP per QD was only ~6 (Fig. 2c, black and red curves) and that there were only 1.73 Alexa594 dyes per QD with a 1 : 4 QD to Alexa594 dye reaction ratio (Fig. 2c, blue curve). Considering the much higher molecular weight of mSA (~53 kDa, Fig. 3b) and the 1 : 1 or 1 : 2 QD to mSA reaction ratio, the majority of mSA–QD conjugates must have had an average binding valency of <1.73 per QD, containing a significant portion of monovalent QDs. We next tested the function of these QDs in staining biotinylated red blood cells (RBCs).[43] The QD staining was specific and could be completely blocked by pre-incubation with small biotin molecules (Fig. 3b). Nonspecific binding was undetectable as the staining pattern of the blocked QDs was indistinguishable from that of the unstained RBCs. The high specificity was verified using single-cell fluorescence microscopy (ESI Fig. 4†) and single-molecule microscopy (ESI Fig. 5†). Binding specificity is critical to many biological applications, in particular to the broad field of single-molecule research that greatly benefits from the unparalleled brightness and photostability of QDs. The presence of the PEG groups on the nanoparticle surface improves specificity in general,[44,45] but the specificity of our QDs exceeds that of previous PEG-containing PIL-passivated QDs that have shown a negligible nonspecific binding.[28,46] Here, we have banished nonspecific binding by minimizing the number of amines to 5% of PIL and by increasing the amine conversion yield.

Secondly, to test the flexibility of our bioconjugation strategies, we used a similar method to make stable, small, specific, low-valency QDs (Fig. 3c). Our strategy was to use a

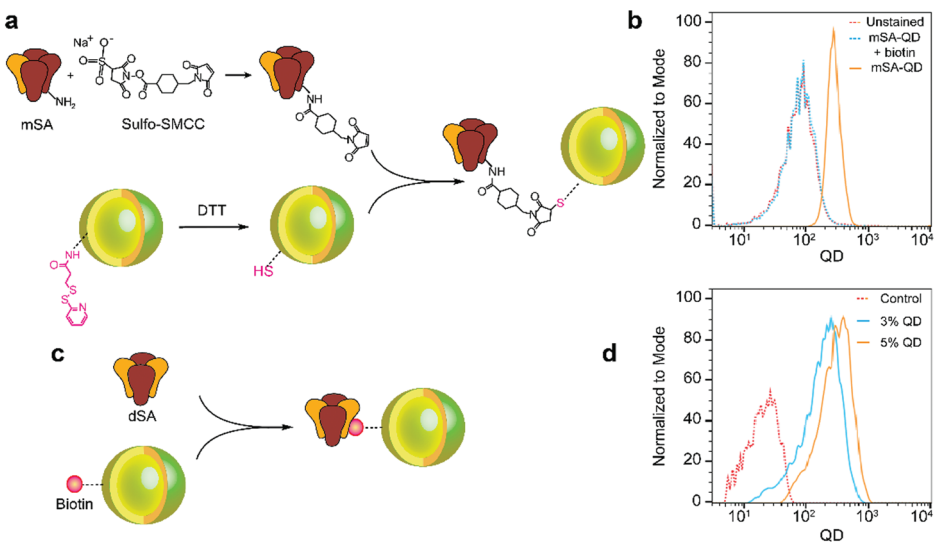

Fig. 3 Specific cell staining by QDs. (a) Schematic showing the mSA and QD conjugation strategy. Thiols on the QDs were exposed by reducing pyridyldithiol groups with DTT and were reacted with maleimide-conjugated mSA. (b) Specific staining of biotinylated RBCs with mSA–QDs validated by flow cytometry. The orange histogram represents specific staining, and the red and blue dotted histograms represent unstained RBCs and the blockage of mSA–QD staining by incubating mSA–QDs with excess biotin beforehand, respectively. (c) Schematic showing the dSA and biotin–QD conjugation strategy. A biotin–QD binds to a dSA and forms a dSA–QD. (d) Specific staining of biotinylated RBCs by dSA–QDs validated by flow cytometry. The blue and orange histograms represent the specific staining of 3% and 5% biotin–QD constructs conjugated to the dSA. The red dotted histogram represents the control staining by biotin–QDs alone.

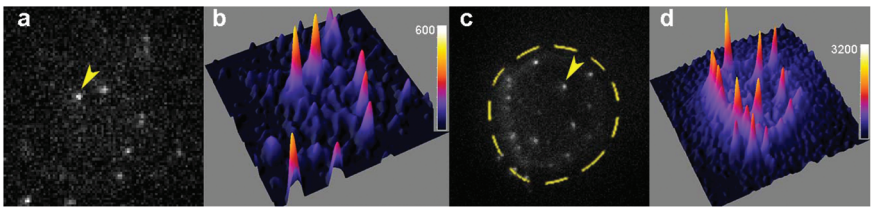

Fig. 4 Single-molecule imaging of homemade specific, compact, low-valency QDs. (a) Imaging single QDs on a glass coverslip. Single QDs were excited with a 488 nm laser and imaged with a 10 ms exposure. The "on" and "off" blinking properties of single QDs on a glass coverslip proves single particle detection (ESI Video S1†). Result is from one representative experiment out of 23 experiments. The arrow indicates one representative single QD. (b) Single QD detection on the glass surface shown by an interactive 3D surface plot using ImageJ. (c) Imaging single QDs on the live cell membrane. Single QDs at the membrane of a CH27 cell were excited with a 488 nm laser and imaged with a 50 ms exposure. Reduced blinking of single QDs was observed at the cell membrane (ESI Video S2†). Result is from one representative experiment out of 20 experiments. The arrow indicates one representative single QD; the yellow dashed line indicates the cell boundary. (d) Single QD detection at cell membrane shown by an interactive 3D surface plot using ImageJ.

dSA to bridge a biotin–QD and a biotinylated POI.[43] We named it dSA–QDs, in parallel with mSA–QDs, although they had the same low binding valency. To make dSA–QDs, the synthesized biotin–QDs were mixed with dSA using a 1 : 1 molar ratio. One alive subunit of dSA is used to bind to the biotin–QDs and the other remaining alive subunit is used to label the targeted POI. After simple incubation and FPLC purification, low-valency dSA–QDs were used to stain biotinylated RBCs.[43] The staining was specific and no staining was observed for biotin–QDs without dSA conjugation (Fig. 3d, dashed, control). As expected, we also found that 5% dSA–QDs produced a slightly stronger staining signal than the 3% dSA–QDs (Fig. 3d, blue and orange lines). The data suggest that our synthesis strategy is reliable, tunable and flexible. We can readily make QDs with different valencies by simply changing the percentage of amines on the QDs. We called this method smart labeling biology, which is simple, straightforward and easy to use in many biological applications.

Application of homemade QDs in single-molecule microscopy

After demonstrating the targeting specificity of our constructs in flow cytometry, we further tested the usage of our homemade mSA–QDs in single-molecule microscopy. We first attached individual QDs onto a biotin-poly-lysine coated glass coverslip and visualized single QD fluorescence using 488 nm laser excitation. Individual QDs were easily detected by an ultra-sensitive electron-multiplying charge-coupled device (EMCCD) camera (Fig. 4a). The intensity profiles of single QDs on the glass surface were further shown by a 3D surface plot (Fig. 4b). Single QDs showed typical blinking behavior (ESI Video S1†), which proved the successful detection of single QDs. Furthermore, we used our homemade QDs to label biotinylated peptide-major histocompatibility complexes (pMHCs) on the CH27 cell surface at a very low molecular density.[47] CH27 is a mouse B-cell lymphoma cell line that expresses I-E^k MHC, which is loaded with biotinylated moth cytochrome C (MCC) peptides to form pMHC molecules.[47] We easily labeled, identified and visualized single pMHC molecules at the live cell membrane (Fig. 4c). The intensity profiles of single QDs at the cell membrane were also clearly shown by a 3D surface plot (Fig. 4d). We found that the blinking of QDs was significantly suppressed on the CH27 cell membrane compared to on the glass surface (ESI Video S2†), consistent with previous reports showing that QD blinking was suppressed when tracking vesicles in the neural synapse[48] and imaging pMHCs in the immunological synapse.[47] This natural suppression of QD blinking at the cell membrane facilitates the tracking of single-molecule events under physiological conditions without using chemicals such as β-mercaptoethanol, which can be harmful to biological samples.[49] Here we show a typical example of tracking a single pMHC trafficking on the CH27 cell surface (ESI Video S3†) with a good spatiotemporal resolution (~30 nm and ~50 ms). Single-molecule labeling was confirmed by checking the blinking profile of a QD-labeled molecule at the live cell membrane (ESI Fig. 6†). In this particular experiment, we used stream mode to continuously image the QDs for ~50 seconds. When used in other biological imaging applications, the time length for which these QDs can be imaged will depend on factors such as the laser intensity, wavelength, exposure time, frame rate and microscopy settings.[47,50–52] Overall, the stable, small, specific, low-valency QDs demonstrated here can be used to label and track a wide variety of biomolecules with minimal perturbation and with high brightness and stability.

Conclusions

We have developed a new method to generate activable, water-soluble, compact QDs with a small number of conjugation handles for long distance delivery, subsequent biomolecule conjugation and single-molecule imaging. The conjugation chemistry is straightforward, flexible, controllable and compatible with different molecules. We have successfully conjugated small organic dyes and chimeric streptavidin proteins to the QDs, yielding stable (covalent conjugation), small (~10–12 nm hydrodynamic diameter), specific (non-detectable nonspecific binding), and low-valency (<1.73) QDs. Such conjugation chemistry can easily be extended to other biomolecules such as antibodies, peptides, oligonucleotides, and lipid molecules

with simple modifications. We further tested the applications of streptavidin–QD conjugates in flow cytometry and single-molecule microscopy, and they showed highly specific labeling, stable binding, and bright fluorescence. The techniques, reagents and concepts developed in this project can be broadly useful for a large variety of biological applications involving labeling, detection and measurement of single cells and single molecules *in vitro* and *in vivo*.

Materials and methods

Materials for QD synthesis

All chemicals were obtained from Sigma Aldrich or Thermo Fisher Scientific and used as received unless indicated otherwise. Air-sensitive materials were handled in an Omni-Lab VAC glovebox under a dry nitrogen atmosphere with oxygen levels <0.2 ppm. All solvents were spectroscopic or reagent grade. Aromatic ring-bearing compounds were visualized by thin layer chromatography using a hand-held UV lamp and $KMnO_4$. Amine-bearing compounds were visualized by thin layer chromatography using a ninhydrin stain. Flash column chromatography was performed on a Teledyne Isco Combi Flash Companion. Size-selective chromatography was performed on GE Healthcare PD-10 columns.

QD and ligand synthesis

CdSe/CdS core–shell quantum dots and PILs were synthesized according to previous reports.[28] The PILs used throughout this work consisted of 50% methoxy-terminated poly(ethylene glycol)$_{11}$ sidechains ($mPEG_{11}$), 5% amine-terminated poly(ethylene glycol)$_8$ sidechains ($AminoPEG_8$), and 45% histamine sidechains.

PIL activation

50% $mPEG_{11}$/5% $AminoPEG_8$/45% histamine-PILs were stirred with SPDP (3.5 eq. of amine) in dimethylformamide (DMF) at room temperature overnight. NHS by-products were removed by sequential addition of solvent, centrifugation, and removal of pellets, using methanol and chloroform as solvents. The activated PIL was then purified by size-selective chromatography in DMF followed by evaporation of DMF and filtration in chloroform.

QD ligand exchange with activated PILs for water-solubilization

The native hydrophobic trioctyl phosphine and trioctyl phosphine oxide NC ligands were displaced by PILs following a previously described procedure.[28] Briefly, CdSe/CdS core–shell quantum dots in trioctylphosphine/octadecene were precipitated with acetone and ethanol. After centrifugation, the supernatant was discarded and the pellet was re-dispersed in chloroform. This solution was added to PILs in chloroform under stirring. After 10 minutes, methanol was added and stirring continued for another 30 minutes. After this time, the solution was diluted with an ethanol/chloroform mixture (1 : 1 v/v) and precipitation was induced by the addition of hexane. The nanoparticles were collected by centrifugation, and the supernatant was discarded. The resulting product was dissolved in water, filtered through a 0.2 μm HT Tuffryn membrane and dialyzed against phosphate-buffered saline (PBS) (pH 7.4). The concentration of the recovered solution was determined by UV-Vis spectroscopy.

Streptavidin mutation, production and purification

A QuickChange kit (Agilent Technologies) was used to insert a TEV cleavage sequence (ENLYFQG) preceding the 6×His-tag of the original alive streptavidin subunit[53] using a two-stage PCR protocol.[54] The PCR products were transfected into XL10-Gold ultracompetent cells by following the manufacturer's instructions. Briefly, 100 μL of cells were thawed and added with 4 μL β-mercaptoethanol mix and 2 μL PCR product into a 14 mL BD Falcon polypropylene round-bottom tube. The tube was heat-pulsed in a 42 °C water bath for 30 seconds and incubated on ice for 2 minutes. 0.9 mL of preheated (42 °C) NZY^+ broth was then added and the tube was incubated at 37 °C for 1 hour under shaking at 250 rpm. 200 μL of the transformation mixture was spread on a LB-ampicillin agar plate and incubated at 37 °C overnight. Six single clones were picked and cultured in LB overnight. The cultured cells were spun down and collected. The DNA was purified using a QIAprep Spin Miniprep Kit. Sequencing of purified DNA confirmed the correct insertion of the TEV cleavage sequence. The amino acid sequence of the alive subunit is as follows: A E A G I T G T W Y N Q L G S T F I V T A G A D G A L T G T Y E S A V G N A E S R Y V L T G R Y D S A P A T D G S G T A L G W T V A W K N N Y R N A H S A T T W S G Q Y V G G A E A R I N T Q W L L T S G T T E A N A W K S T L V G H D T F T K V K P S A A S E N L Y F Q G H H H H H H.

We followed the protocol of Alice Ting *et al.* to express and refold the streptavidins,[55] and we used a two-stage imidazole gradient elution protocol to purify the chimeric streptavidins.

Streptavidins with different valencies were made by mixing alive subunits (A) with dead subunits (D) at a 1 : 3 ratio. The protein mixture was first passed through a nickel column to remove waste and most of the D4 streptavidin. After elution by imidazole, the protein mixture was dialyzed using a dialysis kit in PBS overnight. Streptavidins with different valencies were then purified using FPLC with a two-stage imidazole gradient (ESI Fig. 3a†). Four distinct peaks appeared on the chromatogram: D4, A1D3, and A2D2 streptavidins were separated by FPLC and collected in this order as the imidazole concentration was increased slowly to 30%, and the last A3D1 streptavidin portion was eluted as the imidazole concentration was increased more quickly to 100%. A4 streptavidin was too low in abundance (expected abundance = 0.39%) to show up as a peak.

The valencies of the four streptavidin constructs were verified using protein SDS-PAGE before (ESI Fig. 3b†) and after (ESI Fig. 3c†) denaturing the streptavidins.[55] The binding valencies were further verified on agarose gel electrophoresis after conjugating with a 58 bp single strand biotin–DNA (ESI Fig. 3d†). After TEV protease cleavage of the 6×His-tag, the mSA and dSA without a 6×His-tag were purified by nickel resin

respectively. The competence of 6×His-tag cleavage from mSA was verified using protein SDS-PAGE (ESI Fig. 3e†).

Conjugation of mSA to QDs

We dissolved 2 mg of Sulfo-SMCC in 200 μL of fresh water purified by a Milli-Q integral water purification system. We then added 50 μL Sulfo-SMCC into 100 μL mSA (0.5 mg mL^{-1}). We incubated the reaction mixture for 30 minutes at room temperature and removed excess crosslinker by desalting twice with desalting columns equilibrated with PBS/1 mM EDTA. Meanwhile, SPDP–QDs were activated by treating with 50 mM DTT for 30 minutes at room temperature and desalted twice to remove excess DTT. To prevent the formation of disulfide bonds between the exposed thiol groups on neighboring QDs during this process, we used degassed PBS, filled the tube with nitrogen and sealed the tube with Parafilm before starting the reaction. We then mixed the reactive forms of QDs and mSA with a ratio of 1 : 1 or 1 : 2 and incubated the mixture overnight in a 4 °C cold room. Unconjugated mSA was removed by size exclusion chromatography on S200 resin.

Testing of QD labeling by flow cytometry

All animal procedures were performed in accordance with the Animal Use Policies and Guidelines at the University of Chicago and approved by the Institutional Animal Care and Use Committee. Mouse RBCs were isolated from mouse whole blood according to an approved Animal Care and Use Protocol. In brief, a mouse was sacrificed and 1 mL of whole blood was collected using a sterile tube containing EDTA. The blood was then carefully layered over 1 mL of Histopaque (Sigma-Aldrich), centrifuged and washed five times with PBS. Isolated RBCs were biotinylated through the amine groups of the cell surface proteins using Biotin-X-NHS (Calbiochem) according to the manufacturer's instruction.[43] Biotin-X-NHS served to couple biotin to the primary amino groups of proteins expressed on the RBC surface under mild alkaline conditions. In brief, RBCs were incubated with titrated Biotin-X-NHS at pH 7.2 for 30 min at room temperature, and washed five times with PBS/1% BSA to remove excess Biotin-X-NHS and stop the reaction. Biotinylated RBCs were stained with 20 nM mSA–QD or dSA–QD conjugates in the presence or absence of 2 mM free biotin molecules. After three washes, the RBCs were analyzed by using an LSR-II flow cytometer (BD).

Cell culture and single-cell imaging

CH27 cells (a B-cell lymphoma cell line) were maintained in complete medium (RPMI 1640 medium, 10% fetal calf serum, 2 mM L-glutamine, 50 μM β-mercaptoethanol and penicillin/streptomycin). CH27 cells express I-E^k MHC molecules and served as the antigen-presenting cells (APCs). The biotin–MCC (88–103) peptide (*i.e.*, the antigen) was custom synthesized and purified by Elim Biopharm. The peptide consisted of a biotin flexible linker and a peptide sequence, biotin-AHX-SGGGSGGGANERADLIAYLKQATK. Underlined residues were synthesized as D-stereoisomers to avoid possible proteolytic cleavage of residues extending outside the MHC binding groove. This extended uncleavable flexible linker provided the space and flexibility for subsequent QD labeling.[16]

APCs were pulsed with 50 nM of biotin–MCC peptides.[47] The peptide-pulsed APCs were washed five times using cold PBS supplemented with 2% BSA and 0.05% NaN_3 (to prevent any possible internalization or export of MHC), resuspended in 1 mL of the same medium and labeled with mSA–QD conjugates at 4 °C for 30 minutes. After five washes, the cells were imaged with a Zeiss microscopy imaging system equipped with an Axio Observer Microscope body, a Zeiss 100× oil objective (numerical aperture 1.45), a nanofocusing z-drive, and an Andor's iXon 897 back-illuminated EMCCD that has single photon detection ability combined with >90% quantum efficiency (Andor Technology), a motorized *x*–*y* stage and a 488 nm line laser. For the single-cell and single-molecule imaging experiments, we acquired a differential interference contrast (DIC) exposure and a QD fluorescence image excited by the 488 nm line laser and collected through a single band 586/20 emission filter (Semrock).

Single-molecule microscopy

We tested single-QD fluorescence signals on glass coverslips and on the APC surface. The mSA–QDs were either bound to the surface of a biotinylated poly-lysine coated coverslip or conjugated to the biotinylated MCC peptides loaded onto a CH27 cell surface. With 488 nm line laser excitation and the highly sensitive Andor EMCCD, we readily detected single QD signals with a high signal-to-noise ratio. All the images were taken with the indicated exposure time using the stream-mode of the EMCCD camera.

Conflicts of interest

There are no conflicts to declare.

Acknowledgements

This work is supported by NIH grants R00AI106941 and R21AI120010 and NSF CAREER Award 1653782 (to J. H.). The work also received support from the NIH through grants 5-U54-CA151884-03 (M. G. B.) and 5R01CA126642-02 (M. G. B.). The Biophysical Instrumentation Facility for the Study of Complex Macromolecular Systems (NSF-0070319, NIH GM68762), the DCIF at MIT (CHE-9808061, DBI-9729592) and the NCI through the Cancer Center Support (core) at MIT (P30-CA14051) are also gratefully acknowledged.

References

1 J. Lippincott-Schwartz and G. H. Patterson, *Science*, 2003, **300**, 87–91.
2 J. Zhang, R. E. Campbell, A. Y. Ting and R. Y. Tsien, *Nat. Rev. Mol. Cell Biol.*, 2002, **3**, 906–918.

3 W. C. Chan, D. J. Maxwell, X. Gao, R. E. Bailey, M. Han and S. Nie, *Curr. Opin. Biotechnol.*, 2002, **13**, 40–46.
4 J. K. Jaiswal and S. M. Simon, *Trends Cell Biol.*, 2004, **14**, 497–504.
5 U. Resch-Genger, M. Grabolle, S. Cavaliere-Jaricot, R. Nitschke and T. Nann, *Nat. Methods*, 2008, **5**, 763–775.
6 O. Chen, J. Zhao, V. P. Chauhan, J. Cui, C. Wong, D. K. Harris, H. Wei, H. S. Han, D. Fukumura, R. K. Jain and M. G. Bawendi, *Nat. Mater.*, 2013, **12**, 445–451.
7 X. H. Gao, Y. Y. Cui, R. M. Levenson, L. W. K. Chung and S. M. Nie, *Nat. Biotechnol.*, 2004, **22**, 969–976.
8 O. Chen, H. Wei, A. Maurice, M. Bawendi and P. Reiss, *MRS Bull.*, 2013, **38**, 696–702.
9 H. W. Duan, M. Kuang and Y. A. Wangi, *Chem. Mater.*, 2010, **22**, 4372–4378.
10 B. Dubertret, P. Skourides, D. J. Norris, V. Noireaux, A. H. Brivanlou and A. Libchaber, *Science*, 2002, **298**, 1759–1762.
11 L. Ma, C. L. Tu, P. Le, S. Chitoor, S. J. Lim, M. U. Zahid, K. W. Teng, P. H. Ge, P. R. Selvin and A. M. Smith, *J. Am. Chem. Soc.*, 2016, **138**, 3382–3394.
12 I. L. Medintz, H. T. Uyeda, E. R. Goldman and H. Mattoussi, *Nat. Mater.*, 2005, **4**, 435–446.
13 X. Michalet, F. F. Pinaud, L. A. Bentolila, J. M. Tsay, S. Doose, J. J. Li, G. Sundaresan, A. M. Wu, S. S. Gambhir and S. Weiss, *Science*, 2005, **307**, 538–544.
14 P. Reiss, M. Protiere and L. Li, *Small*, 2009, **5**, 154–168.
15 N. Q. Zhan, G. Palui, J. P. Merkl and H. Mattoussi, *J. Am. Chem. Soc.*, 2016, **138**, 3190–3201.
16 X. Zhang, A. Shamirian, A. M. Jawaid, C. M. Tyrakowski, L. E. Page, A. Das, O. Chen, A. Isovic, A. Hassan and P. T. Snee, *Small*, 2015, **11**, 6091–6096.
17 M. Howarth, W. H. Liu, S. Puthenveetil, Y. Zheng, L. F. Marshall, M. M. Schmidt, K. D. Wittrup, M. G. Bawendi and A. Y. Ting, *Nat. Methods*, 2008, **5**, 397–399.
18 T. Pellegrino, L. Manna, S. Kudera, T. Liedl, D. Koktysh, A. L. Rogach, S. Keller, J. Radler, G. Natile and W. J. Parak, *Nano Lett.*, 2004, **4**, 703–707.
19 A. M. Smith, H. W. Duan, M. N. Rhyner, G. Ruan and S. M. Nie, *Phys. Chem. Chem. Phys.*, 2006, **8**, 3895–3903.
20 V. P. Chauhan, T. Stylianopoulos, J. D. Martin, Z. Popovic, O. Chen, W. S. Kamoun, M. G. Bawendi, D. Fukumura and R. K. Jain, *Nat. Nanotechnol.*, 2012, **7**, 383–388.
21 H. S. Choi, W. Liu, P. Misra, E. Tanaka, J. P. Zimmer, B. I. Ipe, M. G. Bawendi and J. V. Frangioni, *Nat. Biotechnol.*, 2007, **25**, 1165–1170.
22 H. S. Choi, W. H. Liu, F. B. Liu, K. Nasr, P. Misra, M. G. Bawendi and J. V. Frangioni, *Nat. Nanotechnol.*, 2010, **5**, 42–47.
23 Z. Popovic, W. H. Liu, V. P. Chauhan, J. Lee, C. Wong, A. B. Greytak, N. Insin, D. G. Nocera, D. Fukumura, R. K. Jain and M. G. Bawendi, *Angew. Chem., Int. Ed.*, 2010, **49**, 8649–8652.
24 M. V. Kovalenko, L. Manna, A. Cabot, Z. Hens, D. V. Talapin, C. R. Kagan, V. I. Klimov, A. L. Rogach, P. Reiss, D. J. Milliron, P. Guyot-Sionnnest, G. Konstantatos, W. J. Parak, T. Hyeon, B. A. Korgel, C. B. Murray and W. Heiss, *ACS Nano*, 2015, **9**, 1012–1057.
25 J. Owens and L. Brus, *J. Am. Chem. Soc.*, 2017, **139**, 10939–10943.
26 S. Tamang, G. Beaune, I. Texier and P. Reiss, *ACS Nano*, 2011, **5**, 9392–9402.
27 N. Zhan, G. Palui and H. Mattoussi, *Nat. Protoc.*, 2015, **10**, 859–874.
28 W. Liu, A. B. Greytak, J. Lee, C. R. Wong, J. Park, L. F. Marshall, W. Jiang, P. N. Curtin, A. Y. Ting, D. G. Nocera, D. Fukumura, R. K. Jain and M. G. Bawendi, *J. Am. Chem. Soc.*, 2010, **132**, 472–483.
29 N. K. Devaraj, R. Weissleder and S. A. Hilderbrand, *Bioconjugate Chem.*, 2008, **19**, 2297–2299.
30 H. S. Han, N. K. Devaraj, J. Lee, S. A. Hilderbrand, R. Weissleder and M. G. Bawendi, *J. Am. Chem. Soc.*, 2010, **132**, 7838–7839.
31 J. Farlow, D. Seo, K. E. Broaders, M. J. Taylor, Z. J. Gartner and Y. W. Jun, *Nat. Methods*, 2013, **10**, 1203–1205.
32 A. Banerjee, T. Pons, N. Lequeux and B. Dubertret, *Interface Focus*, 2016, **6**, 20160064.
33 H. S. Han, E. Niemeyer, Y. H. Huang, W. S. Kamoun, J. D. Martin, J. Bhaumik, Y. C. Chen, S. Roberge, J. Cui, M. R. Martin, D. Fukumura, R. K. Jain, M. G. Bawendi and D. G. Duda, *Proc. Natl. Acad. Sci. U. S. A.*, 2015, **112**, 1350–1355.
34 P. Zrazhevskiy, M. Sena and X. H. Gao, *Chem. Soc. Rev.*, 2010, **39**, 4326–4354.
35 H. S. Han, J. D. Martin, J. Lee, D. K. Harris, D. Fukumura, R. K. Jain and M. Bawendi, *Angew. Chem., Int. Ed.*, 2013, **52**, 1414–1419.
36 B. A. Kairdolf, M. C. Mancini, A. M. Smith and S. M. Nie, *Anal. Chem.*, 2008, **80**, 3029–3034.
37 D. Mathur, A. Samanta, E. Oh, S. A. Diaz, K. Susumu, M. G. Ancona and I. L. Medintz, *Chem. Mater.*, 2017, **29**, 5762–5766.
38 A. Banerjee, C. Grazon, T. Pons, D. Bhatia, C. A. Valades-Cruz, L. Johannes, Y. Krishnan and B. Dubertret, *Nanoscale*, 2017, **9**, 15453–15460.
39 E. Muro, T. Pons, N. Lequeux, A. Fragola, N. Sanson, Z. Lenkei and B. Dubertret, *J. Am. Chem. Soc.*, 2010, **132**, 4556–4557.
40 E. Giovanelli, E. Muro, G. Sitbon, M. Hanafi, T. Pons, B. Dubertret and N. Lequeux, *Langmuir*, 2012, **28**, 15177–15184.
41 Y. Chen, D. M. Montana, H. Wei, J. M. Cordero, M. Schneider, X. Le Guevel, O. Chen, O. T. Bruns and M. G. Bawendi, *Nano Lett.*, 2017, **17**, 6330–6334.
42 H. Wei, O. T. Bruns, M. G. Kaul, E. C. Hansen, M. Barch, A. Wisniowska, O. Chen, Y. Chen, N. Li, S. Okada, J. M. Cordero, M. Heine, C. T. Farrar, D. M. Montana, G. Adam, H. Ittrich, A. Jasanoff, P. Nielsen and M. G. Bawendi, *Proc. Natl. Acad. Sci. U. S. A.*, 2017, **114**, 2325–2330.

43 J. Huang, V. I. Zarnitsyna, B. Liu, L. J. Edwards, N. Jiang, B. D. Evavold and C. Zhu, *Nature*, 2010, **464**, 932–936.
44 E. L. Bentzen, I. D. Tomlinson, J. Mason, P. Gresch, M. R. Warnement, D. Wright, E. Sanders-Bush, R. Blakely and S. J. Rosenthal, *Bioconjugate Chem.*, 2005, **16**, 1488–1494.
45 B. C. Mei, K. Susumu, I. L. Medintz, J. B. Delehanty, T. J. Mountziaris and H. Mattoussi, *J. Mater. Chem.*, 2008, **18**, 4949–4958.
46 W. Liu, M. Howarth, A. B. Greytak, Y. Zheng, D. G. Nocera, A. Y. Ting and M. G. Bawendi, *J. Am. Chem. Soc.*, 2008, **130**, 1274–1284.
47 J. Huang, M. Brameshuber, X. Zeng, J. Xie, Q. J. Li, Y. H. Chien, S. Valitutti and M. M. Davis, *Immunity*, 2013, **39**, 846–857.
48 Q. Zhang, Y. L. Li and R. W. Tsien, *Science*, 2009, **323**, 1448–1453.
49 S. Hohng and T. Ha, *J. Am. Chem. Soc.*, 2004, **126**, 1324–1325.
50 Y. P. Chang, F. Pinaud, J. Antelman and S. Weiss, *J. Biophotonics*, 2008, **1**, 287–298.
51 F. Pinaud, S. Clarke, A. Sittner and M. Dahan, *Nat. Methods*, 2010, **7**, 275–285.
52 M. A. Walling, J. A. Novak and J. R. Shepard, *Int. J. Mol. Sci.*, 2009, **10**, 441–491.
53 M. Howarth, D. J. Chinnapen, K. Gerrow, P. C. Dorrestein, M. R. Grandy, N. L. Kelleher, A. El-Husseini and A. Y. Ting, *Nat. Methods*, 2006, **3**, 267–273.
54 W. Y. Wang and B. A. Malcolm, *BioTechniques*, 1999, **26**, 680–682.
55 M. Howarth and A. Y. Ting, *Nat. Protoc.*, 2008, **3**, 534–545.